Nonadiabatic quasiparticle approach for rotation-particle coupling in triaxial odd-*A* nuclei

Swati Modi, M. Patial,* and P. Arumugam
Department of Physics, Indian Institute of Technology Roorkee, Roorkee 247667, India

E. Maglione
Dipartimento di Fisica e Astronomia "G. Galilei" and Istituto Nazionale di Fisica Nucleare, Via Marzolo 8, I-35131 Padova, Italy

L. S. Ferreira
Centro de Física e Engenharia de Materiais Avançados CeFEMA and Departmento de Física, Instituto Superior Técnico, Universidade de Lisboa, Avenida Rovisco Pais, P1049-001 Lisbon, Portugal

(Received 24 October 2016; revised manuscript received 11 January 2017; published 27 February 2017)

We discuss the formulation of a nonadiabatic approach to study the rotational states in triaxially deformed odd-*A* nuclei. The rotation-particle coupling is treated microscopically by coupling the triaxial rotor states of the even-even core with the states of the valence particle in order to obtain the matrix elements of the odd-*A* system. We arrive at a nonadiabatic quasiparticle approach where the rotational states can have contributions from various quasiparticle states near the Fermi level. We bring out the advantages of this approach over the conventional particle rotor model with a fixed or variable moment of inertia. One clear evidence favoring our approach is the rotation alignment phenomenon which is demonstrated in the case of ^{137}Pm. We discuss our results for ^{136}Nd and ^{137}Pm, and justify that this approach is suitable also for studying nuclei away from stability.

DOI: 10.1103/PhysRevC.95.024326

I. INTRODUCTION

With the emergence of new experimental facilities, exotic nuclei are becoming more accessible in the laboratory. These exotic nuclei posses several surprising features like the spontaneous emission of proton near the proton drip line [1–4], their astrophysical implications [5–7], the neutron skins and the halos in nuclei near the neutron drip line [8], changing magic numbers [9,10], the island of inversion [11], etc. These features cannot be explained by many of the conventional models. In most cases, for exotic nuclei, the primary observable is the spectrum of a few low-lying rotational states. Most of the structure information is contained in the angular momentum and parity of these rotational states. Experimentally it is a very challenging task, to assign spin and parity by measuring a few transitions only. On the other hand, theoretical spin-parity assignments can be reliable only with a versatile and rigorous formulation, which is capable to study nuclei far from the stability also. With this motivation, we have developed a more microscopic approach to study the low-lying excited states of triaxially deformed odd-*A* nuclei.

The rotational spectrum of an odd-*A* nucleus is a manifestation of various possible angular momentum couplings between the odd (valence) particle and the core (even-even nucleus). In a simpler realization, one can treat the nucleus as a one quasiparticle-plus-rotor system where the rotor could be a rigid one. The conventional particle-rotor model (PRM) based on this idea is widely used to explain the measured spectra [12,13]. While explaining such spectra, several parameters of the PRM are adjusted to have a best fit, limiting the predictability of such an approach. In many realizations of PRM [14,15] the relative energy differences between different band heads are either ignored or unreliable due to changing parameters for the different rotational bands. Consequently, ascertaining the low-lying states is also unreliable. The PRM assumes either fixed or variable moment of inertia (VMI). In most of the cases, the rotor is not so rigid, and hence VMI looks reasonable. However, the realization of VMI is not consistent in many cases as we demonstrate in this work.

It is possible to carry out the rotation-particle coupling by coupling the (experimental) core energies directly with the particle states. We define this as a modified particle-rotor model (MPRM) where the matrix elements (ME) of the rotational Hamiltonian of an odd-*A* nucleus is written in terms of the ME of the rotor states through angular momentum couplings. Initially, such an approach was applied in the coupled channel scattering theory [12] for axially deformed nuclei. The predictive nature of this approach was utilized to study the rotational states built on bound states and narrow resonances in odd-*A* nuclei, and its application to proton emission [16]. This was further extended by considering nonadiabaticity and applied to the calculation of structure and decay properties of axially deformed odd-*A* nuclei [17]. Recently, this approach has been extended to axially deformed odd-odd nuclei as well [18]. For the triaxially deformed nuclei, similar calculations are reported [19], and the extension to study exotic nuclei was realized with adiabatic calculations [20].

In the case of axially deformed nuclei, the ME of the rotor are diagonal and hence can be replaced by the experimental (core) energies. This is not the case in triaxial nuclei and hence to construct the MPRM, one needs to calculate the ME of the rotor utilizing the experimental energies and the theoretical wave functions. For a rigid core, it is reliable to consider the moment of inertia and utilizing the VMI one can take care of

*Present address: Department of Physics, Worcester Polytechnic Institute, Worcester, MA 01609.

 ©2017 American Physical Society

the deviations from rigid behavior as well. In the following section we discuss our theoretical framework comprising the description of different VMI methods for the triaxial rotor, followed by the rotation-particle coupling approaches. Then we discuss our results for ^{136}Nd (rotor) and ^{137}Pm (particle-plus-rotor), to justify our approach and highlight its suitability for studying nuclei away from stability.

II. THEORETICAL FRAMEWORK

It is convenient to follow the developments in the formalism in three parts viz., (i) triaxial rotor, (ii) mean-field experienced by the particle, and (iii) rotation-particle coupling which couples the former two parts.

A. Triaxial rotor

The Hamiltonian for the triaxial rotor is given by

$$H_{\rm rot} = \sum_{k=1,2,3} \frac{\hbar^2}{2\mathcal{I}_k} R_k^2, \tag{1}$$

where $\mathcal{I}_k$ and R_k are the moments of inertia and angular momenta, respectively, in the three directions. The rotor energies are obtained using the relation

$$H_{\rm rot}|RM_Ri\rangle = E_{Ri}|RM_Ri\rangle \tag{2}$$

with the eigenfunctions [21]

$$|RM_Ri\rangle = \sum_{K_R} c^{Ri}_{K_R}|RM_RK_R\rangle, \tag{3}$$

where

$$|RM_RK_R\rangle = \sqrt{\frac{2R+1}{16\pi^2(1+\delta_{K_R,0})}} \times \left[D^R_{M_R,K_R}(\omega) + (-1)^R D^R_{M_R,-K_R}(\omega)\right]. \tag{4}$$

Here, ω represents the orientation of the rotor in the laboratory frame and R is the total angular momentum given by $R^2 = \sum_k R_k^2$. The index M_R and K_R are the projections of R on the third axes in the laboratory frame (the z axes) and intrinsic frame of the rotor respectively. K_R can have all non-negative even integers from 0 to R, but for odd R, $K_R = 0$ is not allowed. The negative counterpart of K_R is degenerate with the positive one. i labels the different eigenstates for a given value of R with $c^{Ri}_{K_R}$ specifying the contribution of each K_R. The spectrum of a triaxial rigid rotor resembles that of an axially deformed rotor with the positive parity ($\pi = +1$) states $R^\pi_i = 0^+_1, 2^+_1, 4^+_1, \ldots$, which is called ground band. The ground band is not very sensitive to the triaxial deformation (represented by the parameter γ). The states $R^\pi_i = 2^+_2, 3^+_1, 4^+_2, 5^+_1, \ldots$ make a single band called γ band which is much sensitive to γ and symmetric about $\gamma = 30^\circ$.

It is well known [22] that the moment of inertia increases with angular momentum which is beyond a rigid-rotor description. In microscopic approaches based on generator coordinate method [23,24] or large scale shell model [25], it is possible to take into account the single-particle, vibrational, and rotational degrees of freedom simultaneously. In such cases, all quantities including the moments of inertia are determined consistently with automatic dependence on angular momentum starting with the given nucleon-nucleon effective interaction. In a phenomenological VMI model, the rotor energies comprise the potential energy $\langle V_k\rangle$ also, which depends on the angular momentum [22]. For such a case, we can write the rotor Hamiltonian as

$$H_{\rm rot} = \sum_{k=1,2,3} V_k + \frac{\hbar^2}{2\mathcal{I}_k} R_k^2 . \tag{5}$$

In this regard several prescriptions can be found in literature. Here we highlight four important methods.

1. Method 1

The potential energy of a rotor can be written as

$$E_{\rm pot} = \tfrac{1}{4}C(\mathcal{I}_1 - \mathcal{I}_{01})^2 + \tfrac{1}{4}C(\mathcal{I}_2 - \mathcal{I}_{02})^2 + \tfrac{1}{4}C(\mathcal{I}_3 - \mathcal{I}_{03})^2. \tag{6}$$

Here, $\mathcal{I}_{01}$, $\mathcal{I}_{02}$, and $\mathcal{I}_{03}$ are the ground state moments of inertia of the asymmetric rotor and the parameter C is the restoring force constant. $\mathcal{I}_{0k}$ and the deformation parameter γ satisfy the relation

$$\mathcal{I}_{0k} = \frac{4}{3}\mathcal{I}_0 \sin^2\left(\gamma - \frac{2\pi k}{3}\right). \tag{7}$$

Here, $\mathcal{I}_0$ is the VMI parameter. The parameter $\mathcal{I}_0$ is proportional to the square of the quadrupole deformation [22,26]. Hence, the ground state moment of inertia $\mathcal{I}_{0k}$ is a function of triaxial (γ) and quadrupole (β) deformations. The potential energy term (6) takes into account the vibrational degrees of freedom. The constants C and $\mathcal{I}_0$ are to be evaluated through a fitting procedure of the experimental energies along with a relation between C, $\mathcal{I}_0$, and $\mathcal{I}_k$. To obtain such a relation, one can utilize the equilibrium condition

$$\frac{\delta E_T}{\delta \mathcal{I}_k} = 0 , \tag{8}$$

where the total energy

$$E_T = \sum_{k=1,2,3}\left[\frac{1}{2}C(\mathcal{I}_k - \mathcal{I}_{0k})^2 + \frac{1}{2\mathcal{I}_k}\langle R_k^2\rangle\right],$$

$$E_T = \sum_{k=1,2,3}\frac{1}{2}C(\mathcal{I}_k - \mathcal{I}_{0k})^2 + \frac{1}{2}\left(\frac{1}{2\mathcal{I}_1} + \frac{1}{2\mathcal{I}_2}\right)\langle R^2 - R_3^2\rangle + \frac{1}{4}\left(\frac{1}{2\mathcal{I}_1} - \frac{1}{2\mathcal{I}_2}\right)\langle R_+^2 + R_-^2\rangle + \frac{1}{2\mathcal{I}_3}\langle R_3^2\rangle. \tag{9}$$

Here, $\mathcal{I}_k$ are the moments of inertia in units of $\hbar^2$. In this formalism, we obtain three separate equations for $\mathcal{I}_k$ from the equilibrium condition (8), so we have to find zeros of each equation at each point in the fitting procedure, rendering it to be numerically intensive.

The value of the parameters C and $\mathcal{I}_0$ can be found by minimizing χ^2, which represents the error in the fit given by

$$\chi^2 = \frac{1}{N}\sum_{\nu=1}^{N}\frac{(E_{\rm exp}(\nu) - E_{\rm the}(\nu))^2}{E^2_{\rm exp}(\nu)}, \tag{10}$$

where N is the number of available experimental energies ($E_{\rm exp}$) and $E_{\rm the}$ is given by Eq. (9). To study the role of γ, we

minimize χ^2 with two parameters C and $\mathcal{I}_0$. For the best fit, γ also is treated as a parameter.

2. Method 2

In an alternative way [27,28], the expression for the moments of inertia can be written as

$$\mathcal{I}_{kRi} = \frac{4}{3}\mathcal{I}_{0Ri}\sin^2\left(\gamma - \frac{2\pi k}{3}\right), \quad \{k = 1,2,3\}. \tag{11}$$

The total energy is given by

$$E_{TRi} = \frac{1}{2}C(\mathcal{I}_{0Ri} - \mathcal{I}_0)^2 + \frac{1}{2\mathcal{I}_{0Ri}}\eta_{Ri}\,, \tag{12}$$

where C and $\mathcal{I}_0$ are the same parameters as described in method 1. $\mathcal{I}_{0Ri}$ are moments of inertia in units of $\hbar^2$ and $\eta_{Ri} = 2\mathcal{I}_{0Ri}E_{Ri}$ is a dimensionless quantity. Applying the equilibrium condition for the total energy, $\partial E_{TRi}/\partial\mathcal{I}_{0Ri} = 0$, we have the desired constraint

$$\mathcal{I}_{0Ri}^3 - \mathcal{I}_0\mathcal{I}_{0Ri}^2 - \frac{1}{2C}\eta_{Ri} = 0. \tag{13}$$

The parameters $\mathcal{I}_0$ and C are evaluated by fitting the theoretical energies E_{TRi} with the experimental energies.

3. Method 3

In this method [19], to obtain the constraint between the constants, the expression for total energy of the triaxial rotor is approximated by the axially deformed rotor's energy [22],

$$E_{TR} = \frac{1}{2}C(\mathcal{I}_{0R} - \mathcal{I}_0)^2 + \frac{1}{2\mathcal{I}_{0R}}R(R+1). \tag{14}$$

Now minimizing this energy with respect to the moment of inertia $\mathcal{I}_{0R}$ ($\partial E_{TR}/\partial\mathcal{I}_{0R} = 0$), we have

$$\mathcal{I}_{0R}^3 - \mathcal{I}_0\mathcal{I}_{0R}^2 - \frac{1}{2C}R(R+1) = 0. \tag{15}$$

The extension to asymmetric rotor can be achieved through the relation

$$\mathcal{I}_k = \frac{4}{3}\mathcal{I}_{0R}\sin^2\left(\gamma - \frac{2\pi k}{3}\right). \tag{16}$$

The parameters $\mathcal{I}_0$ and C are evaluated by fitting the sum of theoretical rotor energies E_{Ri} (2) and the potential energy term given in Eq. (14), with the experimental energies.

4. Method 4

Another widely used VMI parametrization [14,15,29,30] employs the following relation:

$$\mathcal{I}_k = \frac{4}{3}\mathcal{I}_0(R)\sin^2\left(\gamma - \frac{2\pi k}{3}\right),$$
$$\text{where} \quad \mathcal{I}_0(R) = \mathcal{I}_0\sqrt{1 + bR(R+1)}\,. \tag{17}$$

$\mathcal{I}_0$ is calculated using the expression $\frac{1}{2\mathcal{I}_0\sqrt{1+6b}} = \frac{E_{2^+}}{6}$, where E_{2^+} is the experimental energy of the $R_i^\pi = 2_1^+$ state [26]. The rotor's energy has the same form as in Eq. (2). The VMI parameter b is determined by fitting with the experimental energies.

Method 1 is constructed without losing any generality whereas the other three methods are its simplifications. Results from method 2 are quite closer to that of method 1, and numerically easier. Hence we follow method 2 in our further calculations. It is obvious that method 3 is an oversimplification. Method 4 is quite simpler and effective for a rotor but has some severe drawbacks while employed in the rotation-particle coupling as explained later.

B. Mean field of triaxial nuclei

The nucleons move in the mean field potential of the system which can be considered as a sum of the Woods-Saxon potential $V_{\rm WS}(\vec{r},\theta,\phi)$, the Coulomb potential $V_{\rm Coul}(\vec{r},\theta,\phi)$ and the spin-orbit potential $V_{\rm so}(\vec{r},\theta,\phi)$. Thus the total mean field nuclear potential for the deformed nucleus is given by

$$V(\vec{r},\theta,\phi) = V_{\rm WS}(\vec{r},\theta,\phi) + V_{\rm Coul}(\vec{r},\theta,\phi) + V_{\rm so}(\vec{r},\theta,\phi) \tag{18}$$

with

$$V_{\rm WS}(\vec{r},\theta,\phi) = -\frac{V_0\left[1 \pm \kappa\left(\frac{N-Z}{N+Z}\right)\right]}{1 + \exp\{{\rm dist}[r(\theta,\phi),r_s(\theta_s,\phi_s)]/a\}}\,, \tag{19}$$

where V_0 is the depth of the potential, κ represents the strength of the isospin dependence, a represents the surface thickness of the nuclear potential, $+$ and $-$ signs stand for the protons and neutrons, respectively. dist$[r(\theta,\phi),r_s(\theta_s,\phi_s)]$ is the distance between the point $r(\theta,\phi)$ and the nearest point $r_s(\theta_s,\phi_s)$ on the deformed nuclear surface. The deformed nuclear surface is given by

$$R(\theta,\phi) = cR_0\left(\sum_{\lambda=0}^{\lambda_{\rm max}}\sum_{\mu=-\lambda}^{\lambda} a_{\lambda\mu}Y_{\lambda\mu}(\theta,\phi)\right), \tag{20}$$

where $a_{\lambda\mu}$ are the deformation parameters and c is the volume conservation constant. In our calculations, we consider even values of λ and μ with $\lambda_{\rm max} = 4$. This translates to the three deformation parameters β_2, β_4 and γ. The Coulomb and spin-orbit potential can be written as

$$V_{\rm Coul}(\vec{r},\theta,\phi) = e\int_V \frac{\rho(\vec{r}\,')}{|\vec{r} - \vec{r}\,'|}d\vec{r}\,'\,, \tag{21}$$

$$V_{\rm so}(\vec{r},\theta,\phi) = -\frac{\lambda_{\rm so}\hbar^2}{4M^2c^2}\frac{1}{r}\nabla \times\left\{\frac{V_0\left[1 \pm \kappa\left(\frac{N-Z}{N+Z}\right)\right]}{1 + \exp\{{\rm dist}[r(\theta,\phi),r_s(\theta_s,\phi_s)]/a\}}\right\} \times[\vec{\sigma}\cdot[\vec{r}\times\vec{p}]_\mu], \tag{22}$$

where $\rho(\vec{r}\,')$ represents the nuclear charge density with uniform charge distribution. $\lambda_{\rm so}$ and $\vec{\sigma}$ are the strength of the spin-orbit interaction and Pauli spin matrices, respectively. M is the mass of nucleon and $\vec{p}$ is the linear momentum operator. We utilize the universal set of parameters [31] for the mean field potential.

C. Rotation-particle coupling

1. Particle rotor model (PRM)

In a conventional approach to explain the rotational spectra through the rotation-particle coupling, the PRM is widely

used. Most of such formulations assume a constant moment of inertia so that the Hamiltonian can be expanded into different parts which have certain physical meaning like the Coriolis term. This often requires lengthy derivation of matrix elements [32,33], especially in the case of triaxial or odd-odd nuclei. While extending such approaches with the VMI (which depends on the rotor's angular momentum R), to simplify the calculations, instead of $\mathcal{I}(R)$ one calculates $\mathcal{I}(I)$, where the total angular momentum of the nucleus, $\vec{I} = \vec{R} + \vec{j}$ and j is the angular momentum of the particle. For example in the VMI as given by Eq. (17), one directly replaces R with I. This is a practical way because R never appears in the basis of PRM calculations. However, it is obvious that this can lead to spurious R dependence of VMI when j is large.

This problem is circumvented in some of the formulations of PRM [34,35] for the axially deformed odd-A nucleus, as outlined below. The total Hamiltonian of the particle-plus-rotor system is

$$H = H_{\text{part}} + H_{\text{rot}}\,, \tag{23}$$

where H_{part} and H_{rot} are the Hamiltonian corresponding to single-particle and the axially symmetric rotor [deduced from Eq. (5)], respectively. For obtaining the expression of VMI, the rotational energy is approximated as the diagonal part of H_{rot} such that

$$\langle H\rangle = E_T = \langle H_{\text{part}}\rangle + \frac{1}{2}C(\mathcal{I}_{IK} - \mathcal{I}_{0K})^2 + \frac{1}{2\mathcal{I}_{IK}}[I(I+1) + \langle j^2\rangle - 2K^2 + \delta_{K,1/2}a(-1)^{I+1/2}(I+1/2)], \tag{24}$$

where K is the projection of I on the symmetry axis and j is the angular momentum of the valence particle. The decoupling parameter a and $\langle j^2\rangle$ are given by

$$a = -\sum_j (-1)^{j+1/2}(j+1/2)B^2_{j,1/2} \quad \text{and}$$

$$\langle K|j^2|K\rangle = \sum_j B^2_{jK}\, j(j+1),$$

where B_{jK} are the expansion coefficients of single-particle states in the spherical basis. Applying the equilibrium condition for the energy, $\partial E_T/\partial \mathcal{I}_{IK} = 0$, we have the equation for VMI,

$$\mathcal{I}_{IK} = \left\{\frac{1}{2C}[I(I+1) + \langle j^2\rangle - 2K^2 + \delta_{K,1/2}a(-1)^{I+1/2}(I+1/2)]\right\}^{1/3}. \tag{25}$$

Here, C is treated as free parameter and the angular momentum dependence of $\mathcal{I}$ is accurate as long as the approximation for E_T is valid.

In most of the PRM calculations, the aim is to fit the observed rotational spectra and hence all the parameters are adjusted to have the best fit [14,15,35], without any emphasis on the physical significance of those parameters. In such cases the resulting VMI may not explain the rotor spectrum. Beyond this drawback, for a model to be more predictive and reliable, there should not be dependency on the parameters determined entirely by fitting the given spectrum of the particle-plus-rotor system only. In the following section we discuss a more appropriate approach for the rotation-particle coupling wherein the parameters are determined unambiguously in a step-wise procedure utilizing the spectrum of the rotor.

2. *Modified particle-rotor model (MPRM)*

For an odd-A nucleus, the total wave function for a given spin (I,M), position $\vec{r}$ of the particle, and orientation ω of the rotor, can be written in the laboratory system as

$$\Psi_{IM}(\vec{r},\omega) = \sum_{ljR\tau} \frac{\phi^I_{ljR\tau}(r)}{r}|ljR\tau, IM\rangle, \tag{26}$$

where $\phi^I_{ljR\tau}(r)/r$ and $|ljR\tau, IM\rangle$ are the radial and angular parts, respectively, in the R representation. The quantum numbers l and j are the orbital and total angular momenta of the particle, respectively, R and τ are rotational quantum numbers of the rotor. The angular part of the total wave function can be written in the uncoupled representation as

$$|ljR\tau, IM\rangle = \sum_{m_p, M_R} \langle jm_pRM_R|IM\rangle|R\tau M_R\rangle|ljm_p\rangle, \tag{27}$$

where $|ljm_p\rangle$ are the particle wave functions in the laboratory frame and m_p is the projection of j. It is useful to transform the wave function from the R representation to the K representation, where the coupling of wave function is easier. In the K representation, the quantum number τ is identified with the projection K_R of R on the rotor's three-axis [20]. The wave functions of the particle and the rotor [first part of Eq. (4)] can be written as

$$|ljm_p\rangle = \sum_{\Omega_p} D^j_{m_p,\Omega_p}|lj\Omega_p\rangle, \tag{28}$$

$$\langle\omega|R\tau M_R\rangle = \langle\omega|RK_RM_R\rangle = \sqrt{\frac{2R+1}{8\pi^2}}D^R_{M_R,K_R}(\omega), \tag{29}$$

where $|lj\Omega_p\rangle$ are the particle wave functions in the intrinsic frame generated using the mean field potential (18) and Ω_p is the projection of j.

Substituting Eqs. (28) and (29) in Eq. (27), and using the Clebsch-Gordan series ((4.25) of [36])

$$|ljRK_R, IM\rangle = \sqrt{\frac{2R+1}{2I+1}}\sum_{K,\Omega_p}{}' \langle j\Omega_pRK_R|IK\rangle \times\left(\sqrt{\frac{2I+1}{8\pi^2}}D^I_{M,K}|lj\Omega_p\rangle\right). \tag{30}$$

The prime in the summation in Eq. (30) stands for the constraint that $K - \Omega_p$ must be an even integer $(0,\pm2,\pm4,\ldots)$ as per the symmetries of the wave function. Demanding that the wave function should not change due to a rotation of an

angle π about the second intrinsic axis, we shall write Eq. (30) as

$$|ljRK_R,IM\rangle = \sqrt{\frac{2R+1}{2I+1}}\sum_{K,\Omega_p}{}'\langle j\Omega_p RK_R|IK\rangle\sqrt{1+\delta_{K_R,0}} \times\left(\sqrt{\frac{2I+1}{16\pi^2}}\left[D^I_{M,K}|lj\Omega_p\rangle + (-1)^{(I-j)}D^I_{M,-K}|lj-\Omega_p\rangle\right]\right). \quad (31)$$

The term within the parenthesis in above equation can be identified as the wave function of the particle-plus-rotor system in the K representation which can be written as

$$|lj\Omega_p K,IM\rangle = \sqrt{\frac{2I+1}{16\pi^2}}\left[D^I_{M,K}|lj\Omega_p\rangle + (-1)^{(I-j)}D^I_{M,-K}|lj-\Omega_p\rangle\right]. \quad (32)$$

Thus we can derive a transformation between the K and R representations as

$$|ljRK_R,IM\rangle = \sum_{K,\Omega_p}{}' A^{IK}_{j\Omega_p,RK_R}|lj\Omega_p K,IM\rangle \quad (33)$$

with the amplitude

$$A^{IK}_{j\Omega_p,RK_R} = \sqrt{\frac{2R+1}{2I+1}}\langle j\Omega_p RK_R|IK\rangle\sqrt{1+\delta_{K_R,0}}. \quad (34)$$

It can be shown that these amplitudes form an orthonormal transformation between the K and the R representations as given by

$$\sum_{K,\Omega_p}{}' A^{IK}_{j\Omega_p,RK_R}A^{IK}_{j\Omega_P R'K_{R'}} = \delta_{RR'}\delta_{K_RK_{R'}},$$
$$\sum_{R,K_R} A^{IK}_{j\Omega_p,RK_R}A^{IK'}_{j\Omega_{p'},RK_R} = \delta_{\Omega_p\Omega_{p'}}\delta_{KK'}. \quad (35)$$

With this property, an inverse transformation can be obtained as

$$|lj\Omega_p K,IM\rangle = \sum_{R,K_R} A^{IK}_{j\Omega_p,RK_R}|ljRK_R,IM\rangle. \quad (36)$$

This allows us to write the matrix elements as

$$\langle lj\Omega_{p'}K',IM|H_{\rm rot}|lj\Omega_p K,IM\rangle = \sum_{R,K_R,K_{R'}} A^{IK'}_{j\Omega_{p'},RK_{R'}}\langle ljRK_{R'},IM|H_{\rm rot}|ljRK_R,IM\rangle \times A^{IK}_{j\Omega_p,RK_R}. \quad (37)$$

Here, $H_{\rm rot}$ includes both the potential and the rotational energies of the rotor (5). In case of axial symmetry, R is even, $K_R = 0$ and $K = \Omega_p$, hence the above equation reduces to the form given in [16]. In such a case, the matrix elements on the right-hand side correspond to the core spectrum and it is straightforward to obtain the matrix elements of the particle-plus-rotor system. For a triaxial rotor, $H_{\rm rot}$ is not diagonal in the basis $|RK_R,IM\rangle$ because K_R is not a good quantum number. But the eigenvectors can be written in terms of these basis states, as given by Eq. (3) and hence we can write Eq. (37) as

$$\langle lj\Omega_{p'}K',IM|H_{\rm rot}|lj\Omega_p K,IM\rangle = \sum_{R,K_R,K_{R'}} A^{IK'}_{j\Omega_{p'},RK_{R'}}\sum_i c^{Ri}_{K_{R'}}E_{TRi}c^{Ri}_{K_R}A^{IK}_{j\Omega_p,RK_R} = W^{K'K}_{j\Omega_{p'}\Omega_p}, \quad (38)$$

where the matrix element $W^{K'K}_{j\Omega_{p'}\Omega_p}$ is termed as the coupling matrix and the PRM realized through this matrix is termed as modified PRM (MPRM). The relation for coupling matrix does not involve any classical approximation and hence can be regarded as a microscopic approach. E_{TRi} is taken from the experimental data. Alternatively, E_{TRi} can be calculated (12) with the parameters C and $\mathcal{I}_0$ obtained through the experimental data for the core. In most of the cases the fit for ground band is almost exact. However, one cannot use the experimental core energies alone because they are limited and assuming zero or infinite energy for the unavailable states will lead to spurious matrix elements. The coefficients $c^{Ri}_{K_R}$ are obtained by diagonalizing $H_{\rm rot}$ in the R representation. For calculating the matrix elements of $H_{\rm rot}$ in the R representation one needs the moment of inertia. Here it is easy and appropriate to consider VMI because R is defined for the basis states. The input from a phenomenological VMI model enters the coupling matrix through $c^{Ri}_{K_R}$ and the higher states of E_{TRi} for which the data are unavailable. The total Hamiltonian for the particle-plus-rotor system can be written as sum of the intrinsic energy of the valence nucleon $H_{\rm av}$ in the deformed mean field, the pairing interaction given by $H_{\rm pair}$ and $H_{\rm rot}$. Thus

$$H = H_{\rm av} + H_{\rm pair} + H_{\rm rot} \quad (39)$$

with the matrix elements given by

$$\langle q'K',IM|H|qK,IM\rangle = \epsilon_q\,\delta_{KK'}\delta_{qq'} + \sum_{lj\Omega_p\Omega_{p'}} W^{KK'}_{j\Omega_p\Omega_{p'}} \times\int dr\; f_{uv}\;\phi^{IK'*}_{lj\Omega_{p'}}(r)\,\phi^{IK}_{lj\Omega_p}(r)\,, \quad (40)$$

where q specifies the single-particle state. ϵ_q are the quasiparticle energies which are calculated from the single-particle energies e_q, using the Bogoliubov transformation, leading to the relation $\epsilon_q = \sqrt{\Delta^2+(e_q-\lambda)^2}$, where Δ is the pairing gap and λ is the BCS chemical potential of the nucleus. We follow the frozen gap approximation with $\Delta = 12/\sqrt{A}$ MeV which is simpler to extend for exotic nuclei. Calculating Δ with a constant pairing force strength is more appropriate but it relies on the availability of data of neighboring nuclei. $\phi^{IK}_{lj\Omega_p}(r)$ is the single-particle wave function in the intrinsic frame. The BCS occupation probability is given by $V_q^2 = \frac{1}{2}[1-(e_q-\lambda)/\epsilon_q]$ and the probability of unoccupation is defined by the relation $V_q^2 + U_q^2 = 1$. The matrix elements between the particle states are transformed to the matrix elements between the quasiparticle states, through the factor $f_{uv} = (U_qU_{q'} + V_qV_{q'})$. The single-particle energies and the wave functions for the valence particle states are obtained by

diagonalizing $H_{\rm av}$ with the mean field potential (18) in the basis $|lj\Omega_p\rangle$. For consistency, in the PRM calculations we define $H_{\rm part} = H_{\rm av} + H_{\rm pair}$ and consider same mean field with quasiparticles.

III. RESULTS AND DISCUSSIONS

A. Analysis of the parameters of VMI

The parameter $\mathcal{I}_0$ is related to the ground state moment of inertia and proportional to the square of the quadrupole deformation (β^2) [22,26]. However, β does not appear explicitly in our equations because this information is in the energy levels used for the fitting. In a simple rotor case, $\mathcal{I}_0$ can be directly related to E_{2^+} like the case of method 4. The three components of moment of inertia follow the hydrodynamical relation defined through γ [Eqs. (7),(11),(16),(17)]. In method 1, the potential energy part has three ground state moments of inertia ($\mathcal{I}_{0i}$) obtained through $\mathcal{I}_0$ and γ [Eq. (7)] and the moments of inertia entering in the kinetic energy part ($\mathcal{I}_k$) are obtained through the equilibrium condition [Eq. (8)]. In the other methods, the ground state moment of inertia has only one value ($\mathcal{I}_0$) and $\mathcal{I}_k$ are evaluated through the hydrodynamical relation [Eqs. (11),(16),(17)]. In all the methods only $\mathcal{I}_0$ and C are fitted with experimental energies. The parameter C is related to the stiffness of the nucleus against vibrational degrees of freedom. Conventionally [22,27], one defines a softness parameter $\sigma = \frac{1}{2C\mathcal{I}_0^2}$. At the limit $C \to \infty$ ($b = 0$ for method 4), all the methods reduce to the rigid rotor form. The difference between methods 1 to 3 vanishes at $\gamma = 0$ and hence these methods yield exactly same C and $\mathcal{I}_0$. These numbers match with those presented in Ref. [22] wherein a wider systematic analysis of these VMI parameters were carried out for the axially deformed nuclei. The reported values of $\mathcal{I}_0$ are in the range 0 to 80 MeV^{-1}. The reported values of σ are typically smaller than unity with exceptionally large values for certain nuclei where the spectra deviate significantly from that of a rigid rotor. For the triaxial case, with calculations similar to our method 2, the VMI parameters are presented in Ref. [27] for selected nuclei with measured rotational spectrum and a γ band. It is reported that the ground band are not sensitive to γ deformation, and hence to obtain best fit at a nonzero γ, the inclusion of γ band is necessary. This is true for a "good" rotational spectrum for which the σ would turn out to be small.

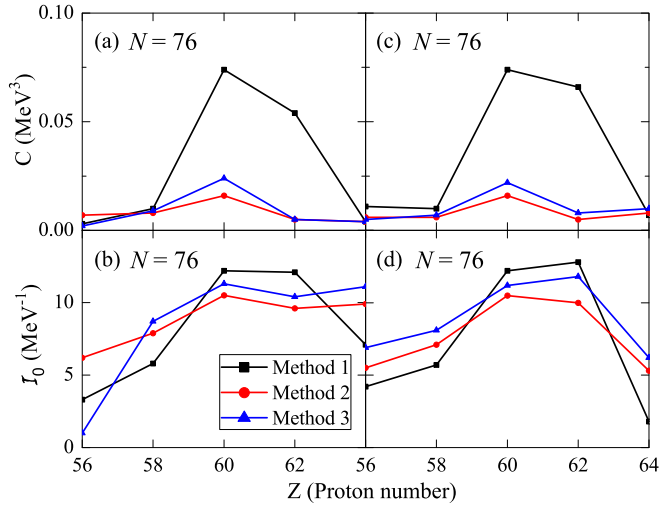

FIG. 1. The VMI parameters C and $\mathcal{I}_0$ for the isotones of $N = 76$ by using methods 1, 2, and 3. In (a) and (b) γ is treated as a free parameter and in (c) and (d) γ is fixed as the value obtained in macroscopic-microscopic calculations [37].

In Table I, we present the VMI parameters for selected nuclei for which the macroscopic-microscopic calculations [37] suggest a strong γ deformation. For the fitting procedure, among the available experimental levels [38] for ground and γ band, the levels with spin up to 10_1^+ and 6_2^+, respectively, are considered. The VMI parameters and γ are varied to obtain the best fit. In Fig. 1 a and b, the VMI parameters from Table I are plotted only for isotopes with neutron number $N = 76$. The VMI parameters can be different for different methods because the form of the total energy of the rotor is different among these methods. Among the first three methods, the results for C from method 1 deviates from the other methods. This is a consequence of the form of the potential energy which has three terms with three moments of inertia in method 1 whereas the other methods have only one term. The parameter

TABLE I. Variable moment of inertia parameters from methods 1, 2, 3 and 4. Among the available experimental levels for ground and γ band, the levels with spin up to 10_1^+ and 6_2^+, respectively, are considered in the fitting.

Nucleus	Z	Method 1			Method 2			Method 3			Method 4	
		C MeV^3	$\mathcal{I}_0$ MeV^{-1}	γ	C MeV^3	$\mathcal{I}_0$ MeV^{-1}	γ	C MeV^3	$\mathcal{I}_0$ MeV^{-1}	γ	b	γ
^{132}Ba	56	0.003	3.3	30.0°	0.007	6.2	36.8°	0.002	1.0	36.5°	0.026	34.3°
^{134}Ba	56	0.004	6.6	30.0°	0.013	4.8	26.6°	0.020	5.7	29.0°	0.027	30.0°
^{134}Ce	58	0.010	5.8	23.3°	0.008	7.9	22.8°	0.009	8.7	23.2°	0.011	34.7°
^{136}Ce	58	0.004	11.3	30.0°	0.021	6.5	26.9°	0.029	7.1	31.3°	0.017	30.0°
^{136}Nd	60	0.074	12.2	25.1°	0.016	10.5	24.3°	0.024	11.3	24.4°	0.008	25.5°
^{138}Nd	60	0.004	9.4	30.0°	0.017	6.9	32.9°	0.016	7.4	34.2°	0.014	30.0°
^{136}Sm	62	0.003	11.7	14.6°	0.003	11.0	15.5°	0.003	10.9	15.3°	0.007	25.1°
^{138}Sm	62	0.054	12.1	17.5°	0.009	11.2	25.1°	0.005	10.4	24.7°	0.028	25.5°
^{140}Gd	64	0.004	7.1	38.6°	0.004	9.9	23.9°	0.004	11.1	24.2°	0.026	25.2°
^{142}Gd	64	0.007	2.1	41.0°	0.004	1.4	37.7°	0.006	2.6	41.5°	0.022	31.1°

TABLE II. Similar to Table I but the triaxial deformation γ is fixed to the value given in Ref. [37].

Nucleus	Z	γ	Method 1			Method 2			Method 3			Method 4
			C MeV^3	$\mathcal{I}_0$ MeV^{-1}	σ	C MeV^3	$\mathcal{I}_0$ MeV^{-1}	σ	C MeV^3	$\mathcal{I}_0$ MeV^{-1}	σ	b
^{132}Ba	56	20.0°	0.011	4.2	0.593	0.006	5.5	0.506	0.005	6.9	0.292	0.135
^{134}Ba	56	30.0°	0.004	6.6	0.438	0.014	4.9	0.296	0.020	5.7	0.134	0.027
^{134}Ce	58	22.5°	0.010	5.7	0.276	0.006	7.1	0.218	0.007	8.1	0.130	0.043
^{136}Ce	58	27.5°	0.002	8.8	0.294	0.021	6.6	0.080	0.026	7.0	0.055	0.020
^{136}Nd	60	25.0°	0.074	12.2	0.004	0.016	10.6	0.026	0.022	11.2	0.015	0.009
^{138}Nd	60	30.0°	0.004	9.4	0.160	0.010	5.9	0.248	0.012	6.6	0.148	0.014
^{136}Sm	62	17.5°	0.003	9.0	0.253	0.003	11.9	0.087	0.004	12.0	0.082	0.020
^{138}Sm	62	22.5°	0.066	12.8	0.003	0.005	10.0	0.094	0.008	11.8	0.039	0.036
^{140}Gd	64	20.0°	0.056	14.7	0.003	0.004	10.4	0.121	0.010	15.1	0.014	0.047
^{142}Gd	64	30.0°	0.002	9.4	0.255	0.008	5.3	0.436	0.010	6.2	0.201	0.022

$\mathcal{I}_0$ (related to the deformation) does not change abruptly with the change in nucleus. The values of C and $\mathcal{I}_0$ are well within the range reported in Ref. [22]. Though the obtained values of VMI parameters are different for different methods, the γ values turn out to be similar. As a next step, to disentangle the effect of change in γ and VMI parameters, we analyze the VMI parameters from different methods for a fixed γ.

In Table II, we present the results for the same set of nuclei presented in Table I but the calculations are done with γ as given in Ref. [37]. The parameters C and $\mathcal{I}_0$ from this table are plotted in panels (c) and (d) of Fig. 1. Some differences in panels (a) and (b) are reduced (for example in case of $Z = 56$ and 58) because of the use of same γ deformation. It has to be noted that the differences in the VMI parameters should not be weighed too much because of the possible coexisting minima in the χ^2 values. In Table II the softness parameter σ is also given, which is inversely proportional to the stiffness parameter C. The parameter b of method 4 can also be considered as a softness parameter. In Fig. 2, the softness parameters of the selected nuclei are plotted versus the proton number Z. All the methods yield same trend of variation of the softness. The nucleus ^{132}Ba has the largest softness among all the other nuclei considered here. This suggests that ^{132}Ba has more vibration like component, i.e., it is less deformed compared to others. As we go beyond ^{132}Ba the deformation increases [37,39]. One can note that for ^{136}Nd the σ is smallest and it originates from a rigid-rotor–like behavior.

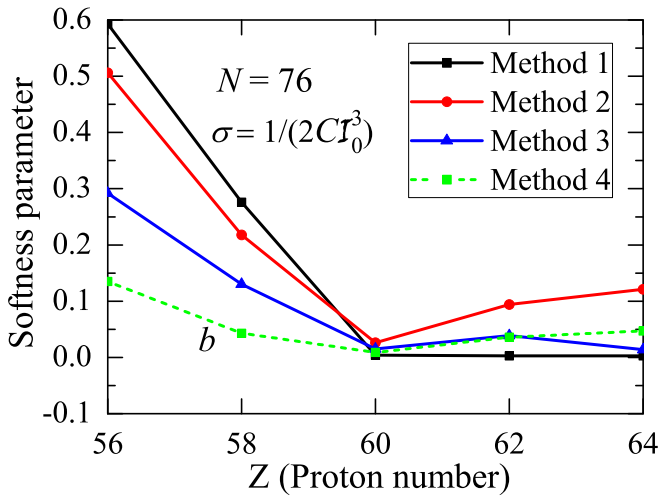

FIG. 2. The softness parameters σ and b obtained from the methods 1, 2, 3, and 4 are shown for the isotones of $N = 76$. This plot is made with Table II. The γ deformation is fixed as the value obtained in macroscopic-microscopic calculations [37].

B. Ground and γ bands of ^{136}Nd

We start our analysis with the triaxial rotor ^{136}Nd. It is predicted to have a triaxial deformation $\gamma = 25°$ according to the macroscopic-microscopic calculations [37], where the macroscopic part is calculated by using the finite-range liquid-drop model (FRLDM) and the microscopic corrections are obtained with the folded-Yukawa single-particle levels. ^{136}Nd is the core for the odd-A triaxially deformed ^{137}Pm ($\beta_2 = 0.190$, $\beta_4 = -0.028$, and $\gamma = 25°$ [37,39]), which is also studied in this work. In Fig. 3, we present the rotational spectrum of ^{136}Nd, calculated with all the four methods described in Sec. II A. The experimental and theoretical results are in very good agreement for the ground band and are quite comparable for the γ band. The calculated γ from all the four methods are consistent with the FRLDM predictions. Both the ground and γ bands are obtained with the same deformation and VMI parameters. The quality of the fit for methods 1 and 2 suggests that both the bands are built on the same configuration [12]. The results from method 3 reveals that the fit for the γ band is not good and so are the underlying approximations of that method. The VMI parameter b dependent method 4 is also somewhat comparable with the other methods.

In Fig. 4, we present the variation of the γ band with the deformation γ. This figure depicts that the γ band appears only for $5° \leqslant \gamma \leqslant 55°$ and it varies swiftly with γ. Thus this band plays a crucial role in determining the triaxiality in nuclei. A common feature of the γ band we can note is that the 2_2^+ and 3_1^+ lie closer and similarly the levels 4_2^+ and 5_1^+ lie closer in contrast to the experimental feature where the 3_1^+ and 4_2^+ lie closer. This feature is inherent to the rigid triaxial rotor model of Davydov and Filippov [26], which can be clearly seen in Fig. 4 b. The extension of this model with VMI also does

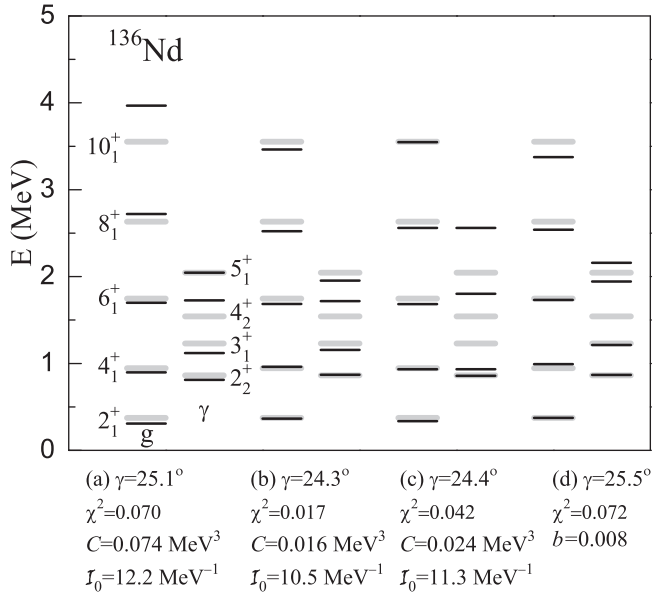

FIG. 3. Rotational spectra of ^{136}Nd for the ground (g) and γ bands. (a), (b), (c), and (d) represent the calculations with methods 1, 2, 3, and 4 for the triaxial rotor as described in Sec. II A. The g band contains only positive parity even angular momentum states, while the γ band contains both even and odd angular momentum states with positive parity. Grey lines correspond to the experimental spectra [40] which are used in the fit. The solid lines represent our calculations with best fitting values of γ and VMI parameters C and $\mathcal{I}_0$ for methods 1, 2, and 3 and parameter b for method 4.

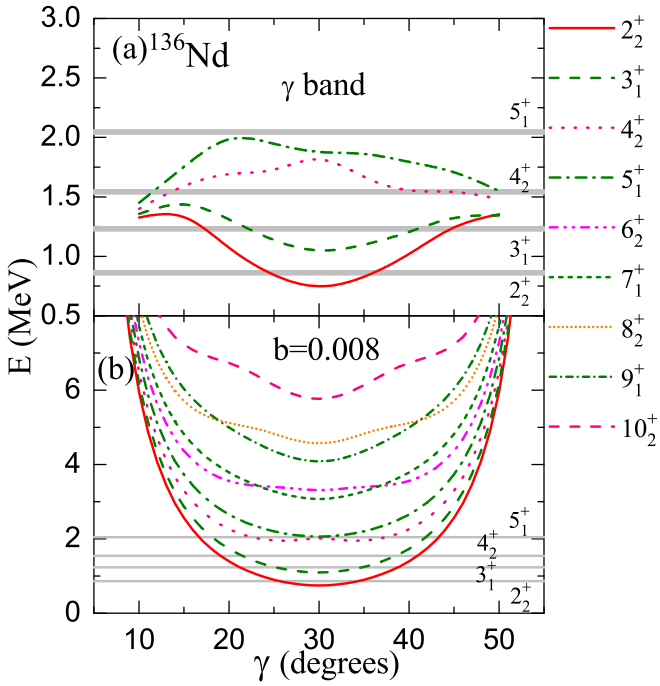

FIG. 4. The γ band of ^{136}Nd calculated with (a) method 2 (Sec. II A 2) and (b) method 4 (Sec. II A 4). Grey lines correspond to the experimental spectra [40].

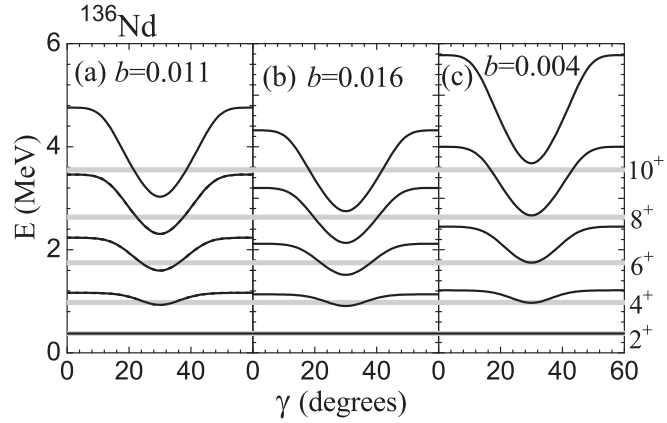

FIG. 5. Energy spectra of ^{136}Nd calculated with different values of VMI parameter b (17).

not affect this feature. This discrepancy regarding the γ band could be attributed to several effects like the mixing of γ band with the two quasiparticle states or other higher vibrational bands, which are neglected in this work.

The rotational spectra for ^{136}Nd obtained with method 4, in which the VMI parameter is represented by b, is presented in Fig. 5 for different values of b. Here only the ground band is considered and we have good fit at different γ depending on the choice of the parameter b. For example, a similar quality fit can be achieved for the combinations (a) $b = 0.011$ and $\gamma \sim 25°$, (b) $b = 0.016$ and $\gamma \sim 20°$, and (c) $b = 0.004$ and $\gamma \sim 30°$. Hence, fixing parameters is quite ambiguous in this method. Apart from this ambiguity propagating to the particle-plus-rotor calculations, this method has serious drawbacks while implementing the VMI as discussed later. However, method 4 (Fig. 5) helps in identifying quickly the significance of triaxiality in even-even nuclei. In our calculations, the parameters fitted to reproduce the rotor spectrum are retained in the particle-plus-rotor calculations as in Refs. [29,30]. This is not the case in many other calculations (e.g., Refs. [14,15]) where all the parameters are tuned freely to fit the spectrum of the odd-A nucleus.

C. Ground and side bands of ^{137}Pm

We proceed to calculate the rotational spectra of odd-A triaxial nucleus ^{137}Pm, in which the measured spectrum of the rotor ^{136}Nd is utilized. The odd proton in ^{137}Pm is coupled with ^{136}Nd through the rotation-particle coupling as discussed in Sec. II C. In Fig. 6, the single-particle (proton) energies and the quasiparticle energies in ^{137}Pm are shown at relevant deformations. In Figs. 6(a), and 6(b), the variation of single-particle and quasiparticle energies is shown as a function of β_2. We choose $\beta_4 = -0.147\beta_2$ predicted by FRDM [39] and hence β_4 is not treated as an independent parameter. The single-particle energy plot provides information about the valence level and the other levels which could contribute to the mixing through the Coriolis interaction. In other words, they help us to identify and restrict the basis states which enter the particle-plus-rotor calculations. The quasiparticle diagram provides a similar information but more accurately.

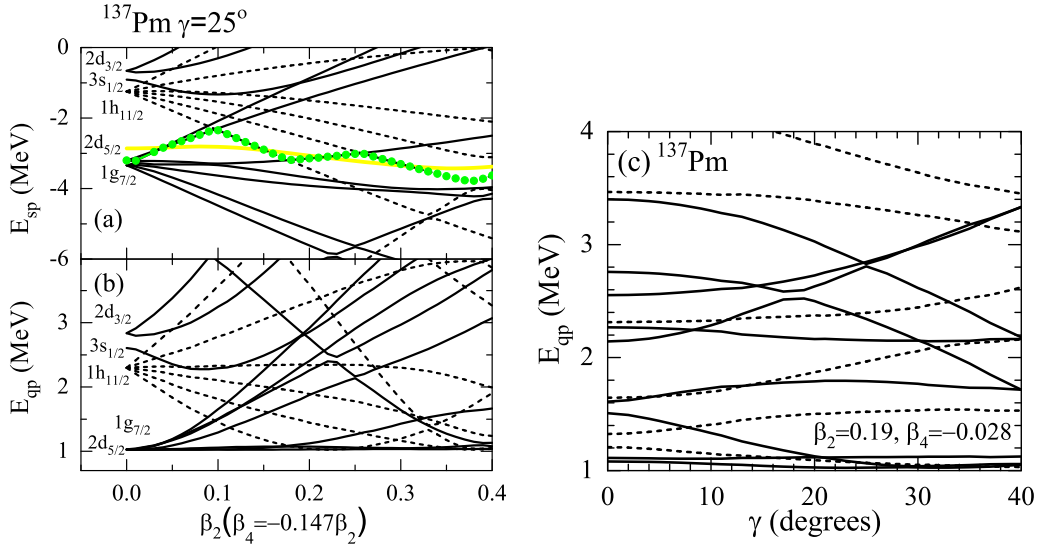

FIG. 6. (a) Single-particle and (b) quasiparticle energies of ^{137}Pm as a function of β_2,(β_4). (c) Quasiparticle energies of ^{137}Pm as a function of γ. These energies are calculated with universal set of parameters [31]. The choice of β_2 and β_4 are consistent with the finite range droplet model calculations [39] and γ is adjusted to have best fit for rotational spectra of ^{136}Nd, which is the core for ^{137}Pm. The solid and dashed lines correspond to the positive and negative parity states, respectively. The green dots represent the states of valence particle and the yellow line represents the chemical potential from BCS calculations. At zero deformation the degenerate states are labeled by l_j.

In Fig. 6(c), we present the variation of quasiparticle energies with the γ deformation. We can note the possibility of change in the yrast state as we go towards higher γ. From these plots, it can be observed that the valence shell (green dots in Fig. 6) may correspond to the different levels originating from the $2d_{5/2}$,$1g_{7/2}$, and $1h_{11/2}$ orbitals. The widely accepted ground state configuration of ^{137}Pm has the valence proton in $1h_{11/2}$ orbital [43,44], and consequently a negative parity yrast band. For highly deformed triaxial shapes, $1h_{11/2}$ orbital can mix (through Coriolis interaction) with the neighboring negative parity orbitals and hence we include the $2p_{1/2}$ and $2f_{7/2}$ orbitals in the basis. Thus all levels of $1h_{11/2}$, $2p_{1/2}$, and $2f_{7/2}$ orbitals are included to form the basis for calculating the matrix elements of the particle-plus-rotor system. This choice assures convergence of our results in terms of the number of basis states.

For the rotation-particle coupling (Sec. II C) we consider three important methods, viz. (i) the PRM with VMI defined through parameter b, (ii) PRM with VMI defined through parameter C (applicable only for axially deformed nuclei), and (iii) MPRM. To highlight the differences in results from these methods, we study the rotation alignment through plots presented in Fig. 7 where only the yrast states are shown. We first discuss the case of $\gamma = 0^\circ$ because the PRM with VMI (25), is applicable for the axially deformed nuclei only. It is conventional [45] in these plots to choose a fixed BCS chemical potential (to see only the role of deformation) far from the valence orbital such that the levels fan out with deformation. Accordingly, in our case the BCS chemical potential $\lambda = -6$ MeV is chosen. In Fig. 7, panel (a) is constructed with the PRM, where rotor is treated as a rigid body. The moment of inertia $\mathcal{I}_0$ is extracted from the $E_{2_1^+}$ (373.7 keV) [40] value of the rotor ^{136}Nd as explained in Sec. II A 4. A well-known feature of the rotation alignment plot is the lowering of the state with $I = 7/2^-$ ($R = 2$) at higher deformations due to the dominance of the deformation alignment [46]. For a demonstration of the method with VMI parameter b, we choose a large value for b(=0.06), and the corresponding results are presented in panel (b). In this procedure, the VMI $\mathcal{I}(R)$ is replaced by $\mathcal{I}(I)$, which leads to the spurious lowering of the higher angular momentum states evidenced clearly in panel (b). In this case we can see,

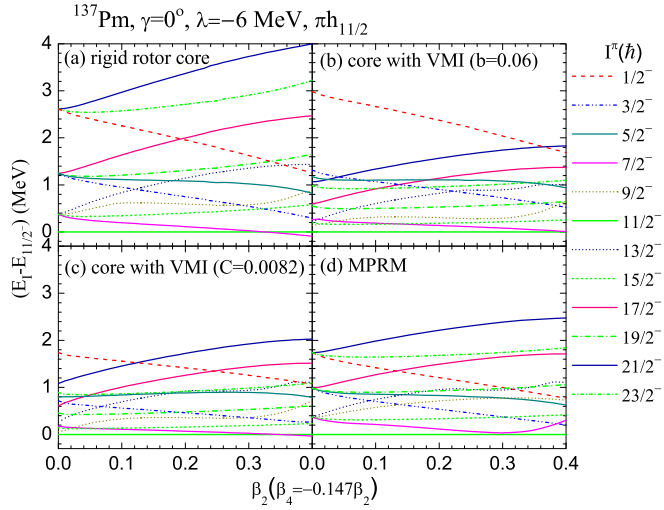

FIG. 7. Spectra showing rotation alignment in ^{137}Pm at $\gamma = 0^\circ$ calculated using different methods with the BCS chemical potential $\lambda = -6$ MeV: (a) PRM with fixed moment of inertia (rigid core). (b) PRM with VMI (17) defined through the parameter b. (c) PRM with VMI (25) defined through the parameter C. (d) MPRM utilizing the experimental energies of the core ^{136}Nd.

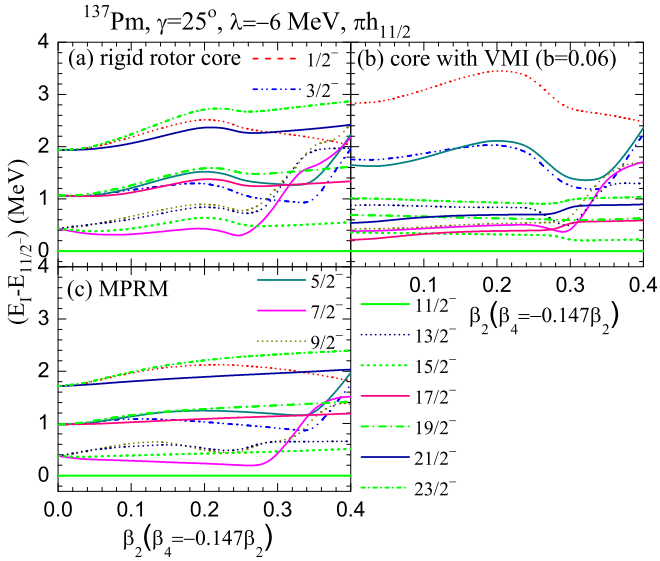

FIG. 8. Similar to Fig. 7, but at $\gamma = 25^{\circ}$.

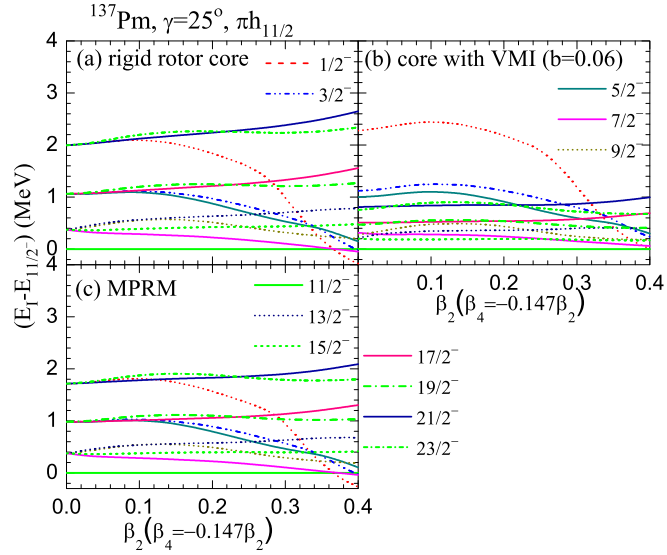

FIG. 9. Similar to Fig. 8, but with the BCS chemical potential calculated at every deformation.

also that, the states with lower angular momentum are pushed upwards. In panel (c), the results are those from the PRM, with VMI (25) depending on parameter C (=0.0082 MeV^3) which fits the rotor spectrum at $\gamma = 0^{\circ}$. Here also one can see that the higher angular momentum states are spuriously lowered but the lower angular momentum states appear as expected. This can be ascribed to the fact that the expression (24) is approximate and is valid for low angular momentum. But in both panels (b) and (c), the degeneracy at zero deformation is not maintained. In panel (d), we present the results from the MPRM. At zero deformation, the particle is completely decoupled and the rotational states have experimental energies of the core ^{136}Nd. Degeneracy at zero deformation is still maintained, we get back the core energies even when the core is not a pure rigid rotor, and there is no spurious lowering of high angular momentum states. In this figure the green lines of different patterns belong to the decoupled band, which is also an important feature of the rotation alignment plot.

The rotation alignment plot for the triaxial deformation $\gamma = 25^{\circ}$ is presented in Fig. 8. A significant change can be observed with the inclusion of γ. The spread in different angular momentum states is now reduced. In panel (a), the PRM comprises the rigid rotor. Panel (b) shows the results of PRM with VMI parameter $b = 0.06$, where the spurious lowering of high angular momentum states and nondegenerate states at $\beta_2 = 0$, are evident. Interestingly, we can note that with the role of triaxial deformation, the role of deformation alignment seems to be attenuated. Here the states corresponding to low angular momentum I are going up at higher β_2 (β_4) instead of coming down. We infer that this is an artifact of having a constant λ. In Fig. 9, a realistic rotation alignment plot is shown where λ is calculated at every deformation. Here we can see that the role of deformation alignment dominates at higher deformation. For a given R, the energies of all the lower angular momentum states rapidly decrease with deformation. This clearly explains the preference for lower angular momentum states in the case of deformation alignment. At higher deformations ($\beta_2 \gtrsim 0.35$) we can see that the $I^{\pi} = 1/2^{-}(R = 6)$ state becomes lower than the expected state with $I^{\pi} = 7/2^{-}$. In all the above rotation alignment plots, we can see that the states which are forming the decoupled band (shown by different green lines) are less affected with the change in β_2.

In Fig. 10 we show the rotational spectra (ground band) of ^{137}Pm as a function of γ. This band is built on one quasiparticle in the $1h_{11/2}$ orbital. The theoretical results are calculated with MPRM utilizing the experimental energies of the core. The core ^{136}Nd is triaxial and hence the corresponding energies comprise the information about γ. Consequently, a major role of triaxiality is already included in the calculation at every γ in terms of the core energies. Thus, in this figure, the rotational energies of the particle-plus-rotor system is not very sensitive to γ. These results conform very well with the experimental data, especially at higher γ where the mean field

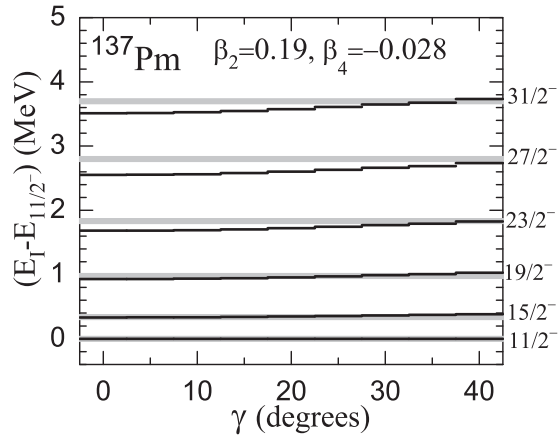

FIG. 10. The ground band of ^{137}Pm calculated with MPRM is plotted with respect to the nonaxial deformation γ. Experimental energies represented by the grey lines are taken from [41,42].

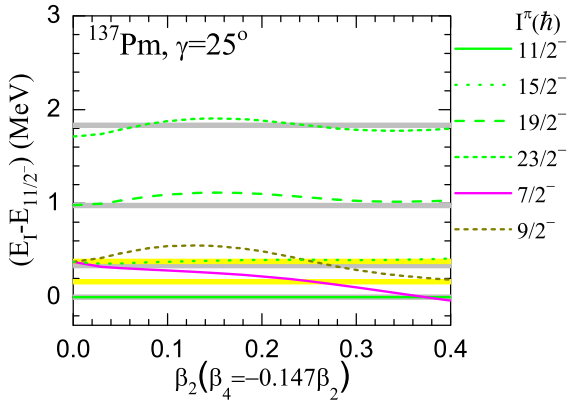

FIG. 11. The ground band along with the states with $I^{\pi} = 7/2^{-}$ and $9/2^{-}$, of ^{137}Pm, calculated with MPRM is presented as a function of the axial deformation $\beta_2(\beta_4)$ where $\gamma = 25^{\circ}$. The thicker lines in grey and yellow colours correspond to the experimental energies of ground and the side bands [41,42], respectively.

of the odd particle also has a triaxial deformation. In Fig. 11, the negative parity ground band along with the states with angular momentum $7/2^{-}$ and $9/2^{-}$ (side band) are shown as a function of $\beta_2(\beta_4)$. The ground band is not very sensitive to β_2 deformation but the side band is quite sensitive to β_2. At $\beta_2 \sim 0.23$, the calculated energies of the side band fits well with the data. The degeneracy of the side band at $\beta_2 = 0$ implies that both these states correspond to $R = 2$. Thus, the state $9/2^{-}$ may not be a simple rotational state built on $7/2^{-}$. These states are favoured by the deformation alignment as shown in Fig. 9. The deformation alignment happens at higher β_2 and hence with increasing β_2 these states are more favoured, as depicted by the lowering of their energies (as seen in Fig. 11 also) at higher β_2.

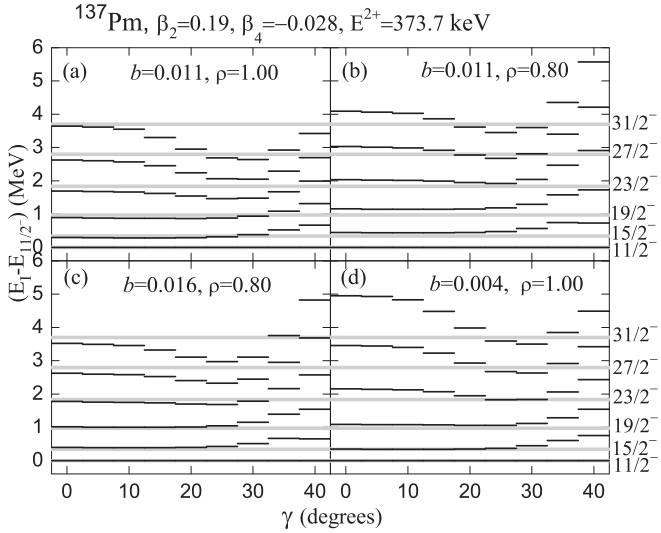

FIG. 12. Ground band of ^{137}Pm calculated within PRM, for different combinations of VMI parameter b, and Coriolis attenuation coefficient ρ. Experimental energies represented by the grey lines are taken from [41,42].

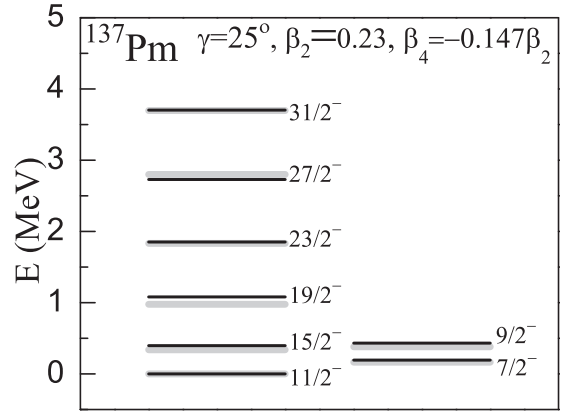

FIG. 13. Low-lying negative parity bands of the odd-A nucleus ^{137}Pm calculated with deformation parameters (β_2, β_4, γ) as mentioned in the inset. Experimental energies represented by the grey lines are taken from [41,42].

In Fig. 12 we present the rotational spectra of ^{137}Pm obtained with the PRM (with VMI parameter b) using different sets of parameters. Here we consider different combinations of two parameters, viz., the VMI parameter b and the Coriolis attenuation coefficient ρ. From Fig. 12, it is clear that with different combinations of parameters, we can obtain fits of similar quality. For example, combinations (a) and (c) favor $\gamma = 0^{\circ}$; (b) favors $\gamma \sim 20^{\circ}$; and (d) favors $\gamma \sim 25^{\circ}$. One can arrive at numerous such combinations while considering b and ρ as free parameters and hence exemplifies their strong influence on the rotational spectrum. Consequently, this method does not yield a unique or unambiguous set of parameters for a given nucleus. These results are quite sensitive to γ because the rotor energies also change swiftly with γ. The change in the rotor energies with γ at the given b, is already shown in Fig. 5.

The best fitting rotational spectrum of ^{137}Pm calculated with MPRM is presented in Fig. 13, which includes the side band also. It is useful to iterate that the parameters C,$\mathcal{I}_0$, and γ are determined from the rotor spectrum. With $\beta_2 = 0.19$ (suggested by FRDM[39]) the calculated ground band energies agree well with the data. In other words, without any adjustable parameters, the MPRM reproduces the ground band. The agreement with the data is better at $\beta_2 = 0.23$ where we get the placement of the side band also correctly, i.e., the relative energy difference between the ground state ($11/2^{-}$) and the $7/2^{-}$ state is in conformity with the experiment. This claim needs to be substantiated by systematic calculations for various similar cases. Identifying the relative placement of bands built on low-lying states is very crucial in the exotic nuclei where only a few levels are identified experimentally. With such validated MPRM, it will be interesting to utilize the resulting wave functions to calculate the decay widths of the proton emitting nuclei.

IV. SUMMARY

We have presented a nonadiabatic approach (MPRM) for the rotation-particle coupling in triaxially deformed odd-A

nuclei. Different methods to study the even-even rotor are analyzed in this regard, with an emphasis on the variable moment of inertia (VMI). From the study of the rotation alignment, we pointed out that the realization of VMI has to be carried out carefully for the rotation-particle coupling. The cases where improper implementation of VMI leads to spurious displacement of rotational states, and ambiguity in parameters, are brought out. We have demonstrated that the MPRM is free from these drawbacks and could even yield the correct relative placement of a side band in ^{137}Pm. This approach is quite suitable to study the low-lying states of the exotic nuclei. Work is in progress to apply this method to study the structure and decay of triaxial proton emitters.

ACKNOWLEDGMENT

This work is supported by the Council of Scientific and Industrial Research, Government of India, via Project No. 03(1338)/15/EMR-II.

[1] B. Blank and M. Borge, Prog. Part. Nucl. Phys. **60**, 403 (2008).
[2] P. J. Woods and C. N. Davids, Annu. Rev. Nucl. Part. Sci. **47**, 541 (1997).
[3] E. Maglione, L. S. Ferreira, and R. J. Liotta, Phys. Rev. Lett. **81**, 538 (1998).
[4] L. S. Ferreira and E. Maglione, Phys. Rev. Lett. **86**, 1721 (2001).
[5] H. Schatz, A. Aprahamian, J. Görres, M. Wiescher, T. Rauscher, J. Rembges, F.-K. Thielemann, B. Pfeiffer, P. Möller, K.-L. Kratz *et al.*, Phys. Rep. **294**, 167 (1998).
[6] M. Hencheck, R. N. Boyd, M. Hellström, D. J. Morrissey, M. J. Balbes, F. R. Chloupek, M. Fauerbach, C. A. Mitchell, R. Pfaff, C. F. Powell *et al.*, Phys. Rev. C **50**, 2219 (1994).
[7] L. S. Ferreira, Jour. of Phys.: Conf. Ser. **580**, 012034 (2015).
[8] I. Tanihata, J. Phys. G Nucl. Phys. **22**, 157 (1996).
[9] D. Steppenbeck, S. Takeuchi, N. Aoi, P. Doornenbal, M. Matsushita, H. Wang, H. Baba, N. Fukuda, S. Go, M. Honma *et al.*, Nature **502**, 207 (2013).
[10] R. V. F. Janssens, Nature **459**, 1069 (2009).
[11] G. L. Wilson, W. N. Catford, N. A. Orr, C. A. Diget, A. Matta, G. Hackman, S. J. Williams, I. C. Celik, N. L. Achouri, H. Al Falou *et al.*, Phys. Lett. B **759**, 417 (2016).
[12] A. Bohr and B. R. Mottelson, *Nuclear Structure*, Vol. II (Benjamin, New York, 1969).
[13] R. F. Casten, *Nuclear Structure from a Simple Perspective* (Oxford University Press, New York, 1990).
[14] G.-j. Chen, Y.-x. Liu, H.-c. Song, and H. Cao, Phys. Rev. C **73**, 034304 (2006).
[15] H. C. Song, Y. X. Liu, and Y. H. Zhang, Chin. Phys. Lett. **21**, 269 (2004).
[16] H. Esbensen and C. N. Davids, Phys. Rev. C **63**, 014315 (2000).
[17] M. G. Procter, D. M. Cullen, M. J. Taylor, G. A. Alharshan, L. S. Ferreira, E. Maglione, K. Auranen, T. Grahn, P. T. Greenlees, U. Jakobsson *et al.*, Phys. Lett. B **725**, 79 (2013).
[18] M. Patial, Ph.D. thesis, Indian Institute of Technology, Roorkee 2013.
[19] H. Toki and A. Faessler, Nucl. Phys. A **253**, 231 (1975).
[20] C. N. Davids and H. Esbensen, Phys. Rev. C **69**, 034314 (2004).
[21] W. Greiner and J. A. Maruhn, *Nuclear Models* (Springer-Verlag, Berlin, 1996).
[22] M. A. J. Mariscotti, G. Scharff-Goldhaber, and B. Buck, Phys. Rev. **178**, 1864 (1969).
[23] J. L. Egido, Phys. Scr. **91**, 073003 (2016).
[24] M. Borrajo and J. L. Egido, Eur. Phys. J. A **52**, 277 (2016).
[25] Y. Tsunoda, T. Otsuka, N. Shimizu, M. Honma, and Y. Utsuno, Phys. Rev. C **89**, 031301(R) (2014).
[26] A. S. Davydov and G. F. Filippov, Nucl. Phys. **8**, 237 (1958).
[27] H. Toki and A. Faessler, Z. Phys. A **276**, 35 (1976).
[28] S. M. Abecasis and E. S. Hernandez, Nucl. Phys. A **180**, 485 (1972).
[29] P. Arumugam, L. S. Ferreira, and E. Maglione, Phys. Rev. C **78**, 041305(R) (2008).
[30] P. Arumugam, L. S. Ferreira, and E. Maglione, Phys. Lett. B **680**, 443 (2009).
[31] J. Dudek, Z. Szymanski, and T. Werner, Phys. Rev. C **23**, 920 (1981).
[32] K. T. Hecht and G. R. Satchler, Nucl. Phys. **32**, 286 (1962).
[33] S. E. Larsson, G. Leander, and I. Ragnarsson, Nucl. Phys. A **307**, 189 (1978).
[34] J. Hastings A. Smith, and F. A. Rickey, Phys. Rev. C **14**, 1946 (1976).
[35] S. Bhattacharya, S. Sen, and R. K. Guchhait, Phys. Rev. C **32**, 1026 (1985).
[36] M. E. Rose, *Elementary Theory of Angular Momentum* (Dover Publications, Inc., New York, 1995).
[37] P. Möller, R. Bengtsson, B. G. Carlsson, P. Olivius, T. Ichikawa, H. Sagawa, and A. Iwamoto, At. Data Nucl. Data Tables **94**, 758 (2008).
[38] Brookhaven National Nuclear Data Center, http://www.nndc.bnl.gov/chart/.
[39] P. Möller, J. R. Nix, W. D. Myers, and W. J. Swiatecki, At. Data Nucl. Data Tables **59**, 185 (1995).
[40] A. A. Sonzogni, Nucl. Data Sheets **95**, 837 (2002).
[41] S. M. Mullins, M. D. Cohler, A. Ghazarian, J. R. Hughes, R. Wadsworth, D. L. Watson, P. J. Bishop, A. J. Kirwan, P. J. Nolan, R. J. Poynter *et al.*, J. Phys. G **14**, 1373 (1988).
[42] E. Browne and J. K. Tuli, Nucl. Data Sheets **108**, 2173 (2007).
[43] C. W. Beausang, L. Hildingsson, E. S. Paul, W. F. Piel, P. K. Weng, N. Xu, and D. B. Fossan, Phys. Rev. C **36**, 602 (1987).
[44] A. Dhal, R. Sinha, D. Negi, T. Trivedi, M. Raju, D. Choudhury, G. Mohanto, S. Kumar, J. Gehlot, R. Kumar *et al.*, Eur. Phys. J. A **48**, 28 (2012).
[45] F. S. Stephens, Rev. Mod. Phys. **47**, 43 (1975).
[46] S. G. Nilsson and I. Ragnarsson, *Shapes and Shells in Nuclear Structure* (Cambridge University Press, Cambridge, 1995).